Chemical Physics Impact 4 (2022) 100079

Contents lists available at ScienceDirect

Chemical Physics Impact

journal homepage: www.sciencedirect.com/journal/chemical-physics-impact

Facile preparation of Nb_2O_5/TiO_2 heterostructures for photocatalytic application

Cátia Liane Ücker [a,*], Fábio Riemke [a], Vitor Goetzke [a], Mário Lúcio Moreira [a], Cristiane Wienke Raubach [a], Elson Longo [b], Sergio Cava [a]

[a] Graduate Program in Materials Science and Engineering, Technological Development Center, Federal University of Pelotas, Gomes Carneiro 1, Pelotas, RS 96010-610, Brazil

[b] CDMF-LIEC, UFSCar, P.O. Box 676, São Carlos, SP 13565-905, Brazil

ARTICLE INFO

Keywords:
Heterostructure
Microwave-assisted hydrothermal
Nb_2O_5/TiO_2
Photocatalysis

ABSTRACT

Nb_2O_5/TiO_2 heterostructure was prepared using the microwave-assisted hydrothermal method and characterized by different techniques. The sample was submitted to a photocatalytic degradation test using the discoloration of rhodamine B under UV-C irradiation for 90 min as a marker. Nb_2O_5/TiO_2 showed an improvement in the photocatalytic benchmark compared to Nb_2O_5, to which it was possible to discolor 100% rhodamine B by essentially a 10% superior output. The samples showed good chemical stability after four different reuse cycles. In addition, the positive charges h^+ were distinguished as the active species that most influenced the photocatalytic performance of the material.

1. Introduction

The incorrect dumping of pollutants by industries in waterbodies directly affects the environment [1,2]. Among the discarded pollutants, we can mention heavy metals [3–5] and organic dyes used by the paint and cellulose industries [1,6,7]. Several technologies have been used for the removal of pollutants found in effluents, such as adsorption [8], heterogeneous photocatalysis [9], membrane separation [10] among others [11]. Heterogeneous photocatalysis is a widely used method that involves the activation of a semiconductor material, originating from pairs of photogenerated charges (electrons/holes - e^- /h^+) that are fundamental to generate radicals with high oxidation power that will be used in the degradation of compounds. organic [12,13].

Niobium pentoxide (Nb_2O_5) is a semiconductor that has great potential for application in heterogeneous photocatalysis due to its interesting characteristics, such as low cost, ease of obtaining, good chemical stability, and wide band gap variations [12,14,15]. However, after excitation of the electron-hole pairs, the semiconductor can present a high recombination rate, limiting its application in photocatalytic processes [16,17]. To improve its photocatalytic behavior, the merging of Nb_2O_5 with another semiconductor material can be an alternative in combination, known as heterostructures [18]. This kind of architecture favors the material's charge segregation and may improve the electronic evolution [19]. Like Nb_2O_5, titanium dioxide (TiO_2) also exhibits reliable chemical stability as a catalyst, with several well-established advantages [20]. In this sense, a mixture of two oxide semiconductors, such as these, may be a good alternative for use in photocatalytic processes to enhance the photocatalytic yield.

The synthesis method to obtain the material can influence the properties of nanoparticles. Microwave-assisted hydrothermal (MAH) synthesis is an effective method for obtaining heterostructures, making it possible to acquire homogeneous and uniform materials at low temperatures and in less time of synthesis when compared to other methods [21,22]. The MAH method has been used to obtain heterostructures involving TiO_2 [23,24] and other systems [25–28]. In different works, heterostructures involving Nb2O5 synthesized by the conventional hydrothermal method [16,29], sol-gel [30,31], freeze-drying [32], among others [33–35] have been found, but not by the MAH method.

Therefore, in this study, we obtained pure Nb_2O_5 and the Nb_2O_5/TiO_2 heterostructure notably faster through the MAH method and administered the materials in heterogeneous photocatalysis tests by checking the discoloration of the rhodamine B (RhB) dye over time.

2. Materials and methods

To obtain Nb_2O_5, $NbCl_5$ (CBMM) was dissolved in 25 mL of distilled

* Corresponding author.
E-mail address: catiaucker@gmail.com (C.L. Ücker).

https://doi.org/10.1016/j.chphi.2022.100079

Available online 26 May 2022

water under constant stirring. Hydrogen peroxide (molar ratio Nb:H_2O_2 was 1:10) was added to the solution, deposited in the microwave reaction cell, and locked up afterward. The synthesis was carried out at a constant temperature of 140°C for 15 min. The resulting material was washed with distilled water and centrifuged to neutralize the pH before the precipitate was oven-dried at 100°C for 12 h. For the Nb_2O_5/TiO_2 synthesis, two solutions were prepared. First, 0.01 mol of titanium isopropoxide was dispersed in 30 mL of ethanol under constant stirring for 10 min. A second solution was prepared, in which 0.01 mol of the obtained Nb_2O_5 was dispersed in 20 mL of ethanol. The two solutions were mixed and transferred to the reaction cell with the synthesis parameters set equal to those for the Nb_2O_5 synthesis.

X-ray diffraction (XRD) analysis was performed using an X-ray diffractometer Bruker (D8 Advance) with CuKα radiation (λ=1.5418 Å). Scanning electron microscopy (SEM) was performed on a JEOL JSM-6610 LV system operating at 15 kV. Transmission electron microscopy (TEM) analysis was performed on a JEM-2100F scanning electron microscope (JEOL, Japan) with a field emission gun (FEG) and an energy-dispersive X-ray spectrometer (EDS) operating at 200 kV. FTIR was obtained with an IR-Prestige (Model 21, Shimadzu, Japan). The diffuse reflectance spectra were obtained by a UV–Vis spectrometer (Varian Cary 5000, USA), and the optical band gap of the samples was estimated by the Wood and Tauc model. Photoluminescence measurements were carried out using a 355 nm laser (Cobolt/Zouk) with the signal detected by a Si-CCD detector (Andor Kymera/Idus).

The photocatalytic process for the samples was analyzed by measuring the discoloration of the RhB [$C_{28}H_{31}ClN_2O_3$] dye in the aqueous solution. For the experiment, 50 mg of the powder was mixed with 50 mL of RhB (1×10^{-5} M) dye under constant stirring to form a solution. The tests were performed in a sealed box under the illumination of five UV-C lamps (15 W each lamp - TUV Philips; maximum intensity at 254 nm) and at a temperature of 25°C. First, all samples were stirred for 15 min in the dark to stabilize the adsorption-desorption equilibrium between the dye and the catalyst. Aliquots were taken at 15 min intervals over the experimental duration of 90 min. All the samples were centrifuged to remove the particulates, and the supernatant was analyzed via UV–vis spectroscopy.

3. Results and discussion

The photocatalytic activities of Nb_2O_5 and Nb_2O_5/TiO_2 were evaluated by discoloration of RhB, according to Fig. 1 (a). The heterostructure Nb_2O_5/TiO_2 showed greater discoloration when compared to Nb_2O_5, in which 90 min it was possible to discolor 100% of RhB, while for Nb_2O_5 it was observed 91%. For comparison, the discoloration behavior of RhB was evaluated using the semiconductor TiO_2 synthesized by the same synthesis method (MAH). TiO_2 showed a very similar behavior to Nb_2O_5, where in 90 min, it was able to discolor approximately 88% of RhB, but it presented a lower result than the heterostructure. This result shows that the junction of the two materials (Nb_2O_5/TiO_2) allows an improvement in the photocatalytic activity through better efficiencies than in relation to the semiconductors alone.

The reaction rate constant (k) of the photocatalytic discoloration process was calculated using the Langmuir-Hinshelwood kinetic method. The kinetic fitting results are shown in Fig. 1 (b), which is in line with a pseudo-first-order reaction. The k values were 0.00174 cm^{-1} for RhB without catalyst, 0.02419 cm^{-1} for TiO_2, 0.02693 cm^{-1} for Nb_2O_5, and 0.4195 cm^{-1} for Nb_2O_5/TiO_2.

The difference in the behavior of the samples can be related to the crystalline phase of the materials, as shown in Fig. 2 (a). The Nb_2O_5 obtained at low temperatures presented the low crystallinity of the pseudohexagonal (TT) phase, according to JCPDS card no. 28-0317, with reference peaks at 22.7°, 26.6°, 34.8°, 46.4°, and 55.6°. For the Nb_2O_5/TiO_2 sample, the diffraction peaks took place at 25.3°, 37.8°, 47.8°, 53.7°, 55.1°, and 62.7°, which is in line with the TiO_2 anatase phase, according to JCPDS card no. 21-1272 mixed with the pseudohexagonal phase of low crystallinity of Nb_2O_5. TiO_2 is a semiconductor material widely used in photocatalysis [36]. Therefore, the mixing of the phases favors the photocatalytic activity, since the mixture of nanostructured oxides can help in more efficient separation of the photogenerated charges because they present a broader light absorption range. Additionally, the heterostructure presented more agglomeration of particles than Nb_2O_5, which may favor the photocatalytic process due to a lower recombination rate, according to Fig. 2 (c) [37]. Nb_2O_5 (Fig. 2 (b)) has homogeneous particles with similar sizes and shapes forming particle aggregates, which are characteristic of the synthesis method (MAH) due to the low temperature and short synthesis time [21]. In the Nb_2O_5/TiO_2 sample, it is possible to verify the presence of smaller particles, characteristic of TiO_2, aggregated together with the Nb_2O_5.

This can be confirmed by the TEM images, as shown in Fig. 3. The image depicted in Fig. 3 (a) presents atoms organized in nanocrystalline domains in which no long-order arrays of atoms can be perceived. This situation is in line with the expected situation for the Nb_2O_5 nanoparticles synthetized at lower temperatures and not subjected to posterior heat treatments [38]. In Fig. 3 (b), the TEM image presents the coexistence of the distinct materials in such a way that the crystalline

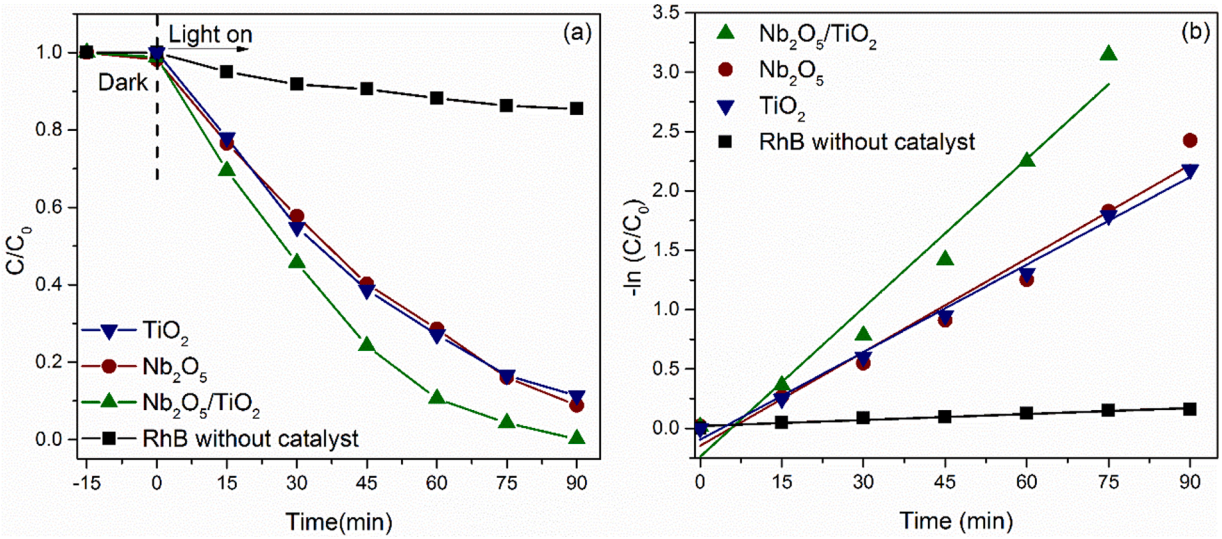

Fig. 1. (a) Photocatalytic activities performance; (b) $-\ln(C/C_0)$ vs. time curve.

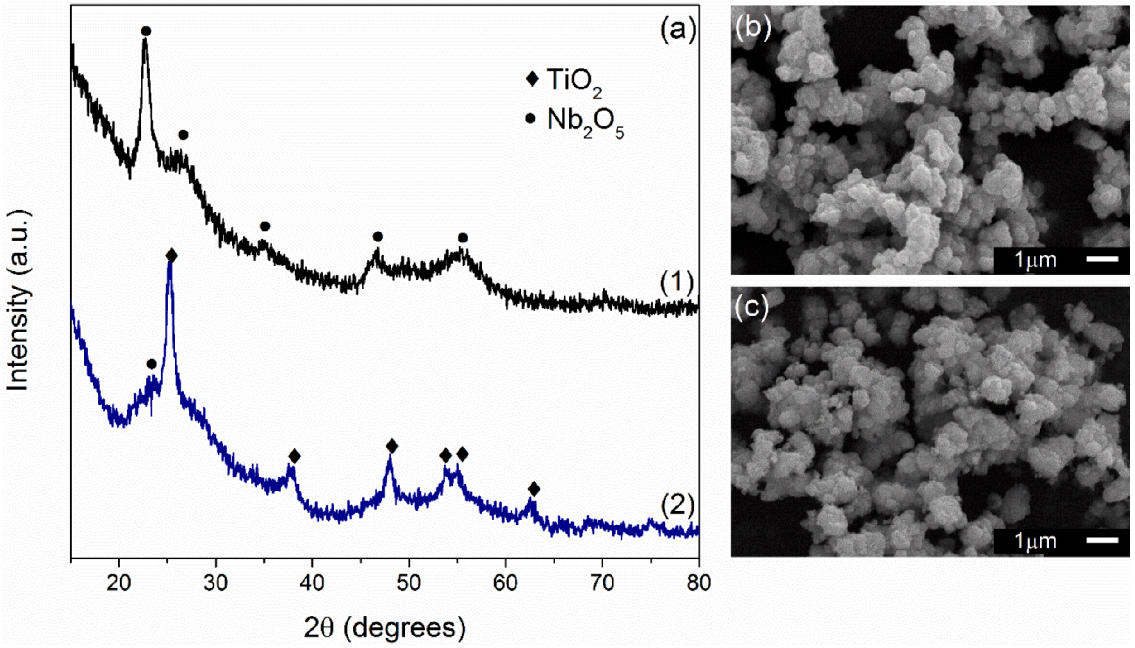

Fig. 2. (a) XRD of the samples: (1) Nb_2O_5 and (2) Nb_2O_5/TiO_2; (b) SEM image of Nb_2O_5; (c) SEM image of Nb_2O_5/TiO_2.

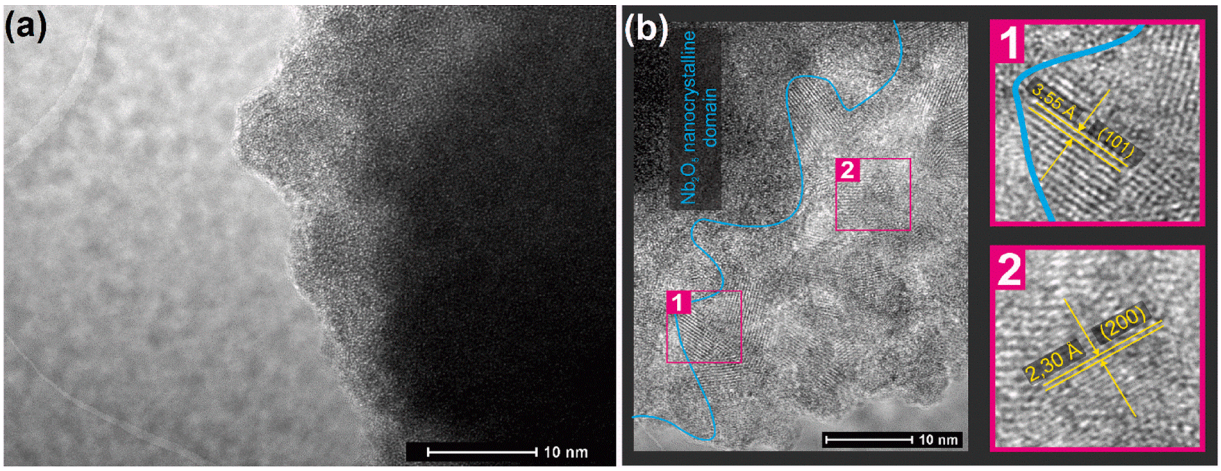

Fig. 3. (a) TEM image for Nb_2O_5; (b) TEM image for the heterostructure Nb_2O_5/TiO_2 with cross-sections zoomed out.

arrays for the anatase phase presented in cross-Sections 1 and 2 are fully integrated into the Nb_2O_5 nanocrystalline clusters with the formation of the niobium matrix on the edge of the TiO_2 crystallites [39]. Such an arrangement may suggest that during the process of synthesis, the TiO_2 and Nb_2O_5 seeds precipitated at distinct stages since the interface within the materials completely isolates the two stoichiometries with no presence of small arrays of one coexisting within the other. In addition, it became evident that the most visible planes for the anatase phase of TiO_2 were the (101) and (200). In addition, both the quantity and arrangement of such orientations denote that the crystallite domains are relatively small, although in line with the expected synthesis at this temperature [40].

Another factor that can influence the photocatalytic performance of a material is the presence of -OH groups [12,41]. FTIR analysis can be used to demonstrate the higher performance of Nb_2O_5/TiO_2 in relation to Nb_2O_5, as shown in Fig. 4 (a). The bands in the regions of 3600 and 3000 cm^{-1} are related to the adsorption of water molecules, and the band at 1630 cm^{-1} corresponds to Ti-OH vibrations [42]. The intensity of these bands is higher for Nb_2O_5/TiO_2 than for Nb_2O_5, which justifies the better photocatalytic performance of the heterostructure, since there was a greater hydroxylation on the surface of the material [43,44]. In addition to these peaks, there are peaks at 1730 cm^{-1}, corresponding to the angular vibration of water molecules, and at 1370 and 1218 cm^{-1}, attributed to the adsorption of O_2 species on the niobium surface [45]. Peaks with low intensity can be seen in bands smaller than 900 cm^{-1}, which are related to typical Nb-O bonds [46].

The band gap can also influence the photocatalytic performance. Fig. 4 (b) and (c) show the band gap of the samples, estimated using the Wood and Tauc model for indirect semiconductors $(\alpha h\nu)^{0.5}$ vs $h\nu$, where α is the absorption coefficient and $h\nu$ is the photon energy in eV. In this analysis, the heterostructure band gap decreased to 3.4 eV compared to the pure Nb_2O_5 sample, which has a band gap of 3.6 eV. This can be attributed to the energies involved in the electronic transitions due to the influence of the TiO_2 nanoparticles, which generally present 3.2 eV as a band gap. These data corroborate the photocatalysis result found in this work, since the Nb_2O_5/TiO_2 sample presented a smaller band gap value than the Nb_2O_5 sample, being able to absorb more light, and consequently, improve the photocatalytic performance.

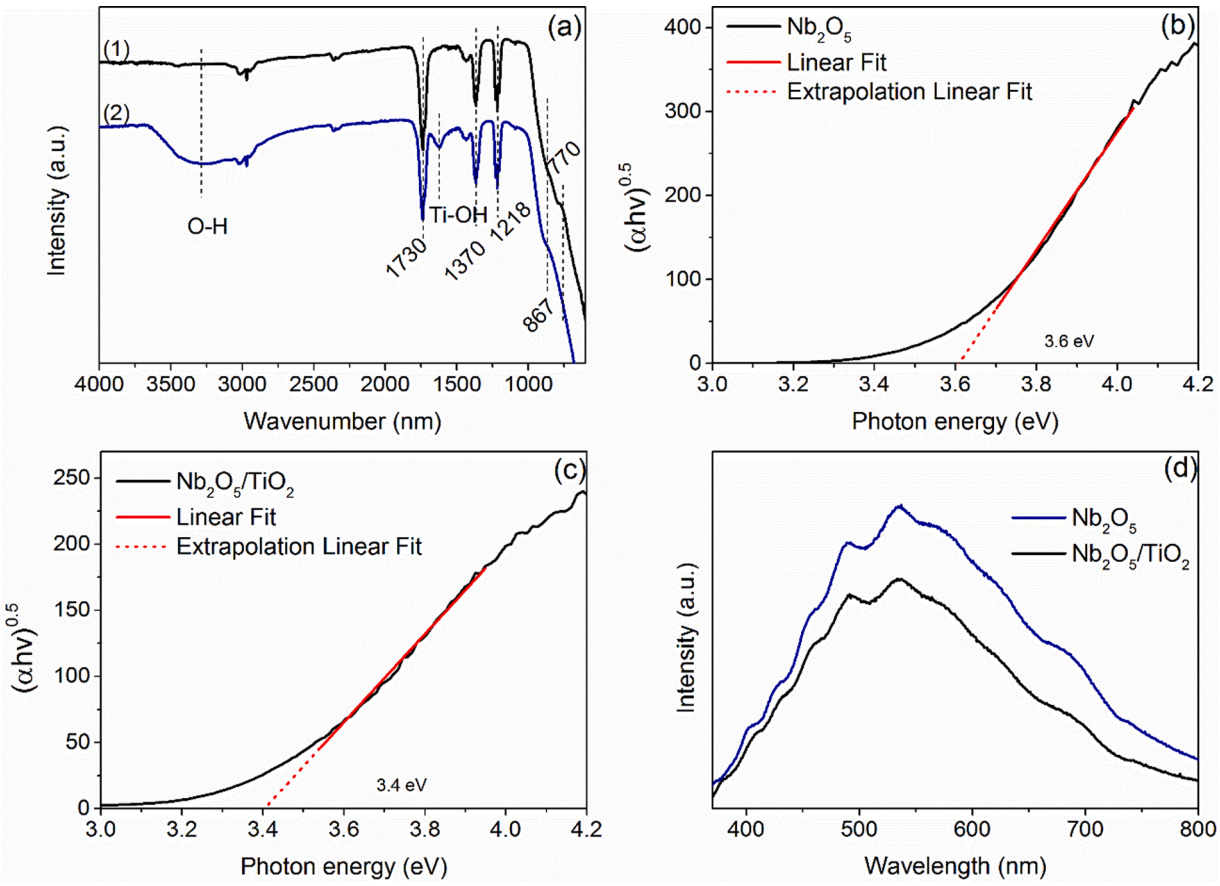

Fig. 4. (a) FTIR spectra of the samples: (1) Nb_2O_5 and (2) Nb_2O_5/TiO_2; (b) band gap energy of Nb_2O_5; (c) band gap energy of Nb_2O_5/TiO_2; and (d) PL spectra of the samples.

The improved photocatalytic performance of Nb_2O_5/TiO_2 in relation to Nb_2O_5 can also be explained by the photoluminescence spectra through the study of the photogenerated charge recombination process of the samples. The spectra of both samples were similar, according to Fig. 4 (d), with two emission peaks centered at 489 and 533 nm, indicating that recombination occurs through a multiphonon process between states located in the band gap of the material, which results in broadband emission [38,47]. The Nb_2O_5 sample exhibited an emission of luminescence with greater intensity, while the Nb_2O_5/TiO_2 heterostructure showed a decrease in intensity. The decrease in heterostructure intensity indicates that the addition of TiO_2 inhibits the charge recombination process, which favors the performance of the photocatalyst, improving the photocatalysis process [48,49].

After justifying the photocatalytic performance of the samples, the chemical stability was analyzed by catalyst reuse over four cycles (Fig. 5 (a) and (b)). After four cycles, both samples showed stability, with performance above 92%, indicating that Nb_2O_5 and Nb_2O_5/TiO_2 were considered stable and highly efficient photocatalysts. To identify the active species in the photocatalytic process, isopropyl alcohol (C_3H_8O), silver nitrate ($AgNO_3$), and disodium ethylenediaminetetraacetate (EDTA) were used as scavengers for ·OH, negative charges (e^-) and positive charges (h^+), respectively. Fig. 5 (c) shows the results of adding scavengers over Nb_2O_5 under UVC irradiation. The addition of EDTA, referring to positive charges h^+, causes a decrease in the photocatalytic efficiency of RhB discoloration when compared to the sample without the addition of scavengers, indicating that h^+ was the main active species during the photocatalysis process. The C_3H_8O also showed a decrease in photocatalytic performance, but more subtly, suggesting that ·OH, even though not the main active species, also helps in the discoloration process of RhB dye. In contrast, the addition of $AgNO_3$ showed an increase in photocatalytic performance when compared to Nb_2O_5 without the addition of scavenger, suggesting that the restriction of e^- leaves a greater number of h^+ available to act in the oxidation of the dye. The same behavior was seen for the Nb_2O_5/TiO_2 sample, as shown in Fig. 5 (d), where h^+ and ·OH were the active species that played the most positive role in the photocatalysis process.

The proposed mechanism to evaluate the photocatalytic activity of the heterostructure is shown below. The valence bands (VB) and conduction band (CB) of semiconductors are important to understand the photocatalytic mechanism. VB and CB can be calculated by Eqs. (1) and (2) [50,51], where E_{VB} and E_{CB} are the VB and CB edge potentials of the semiconductors, E_e is the energy of free electrons on the hydrogen scale (4.5 eV vs NHE – normal hydrogen electrode), X is the average absolute electronegativity (x) of each semiconductor atom ($x_{Nb} = 4.0\ eV$, $x_O = 7.54\ eV$, $x_{Ti} = 3.45\ eV$) [52], and E_g is the band gap of the semiconductors (3.6 eV for Nb_2O_5 and 3.2 eV for TiO_2).

$$E_{VB} = X - E_e + 0.5E_g \quad (1)$$

$$E_{CB} = E_{VB} - E_g, \quad (2)$$

Thus, the calculated values were E_{CB}= -0.01 eV and E_{VB}= 3.59 eV for Nb_2O_5 and E_{CB}= -0.29 eV and E_{VB}= 2.91 eV for TiO_2.

Through the results, the possible S-scheme mechanism of RhB dye discoloration is proposed, according to Fig. 6. With the formation of the heterostructure, changes occur in the photogenerated charge transfer process, where Nb_2O_5 has a more positive VB and CB than TiO_2. This shows that heterostructures make a greater contribution from the availability of tools to the photocatalysis process than do materials that are not heterostructures. When the heterostructure is then excited by photons with energy equal to or greater than the band gap of the

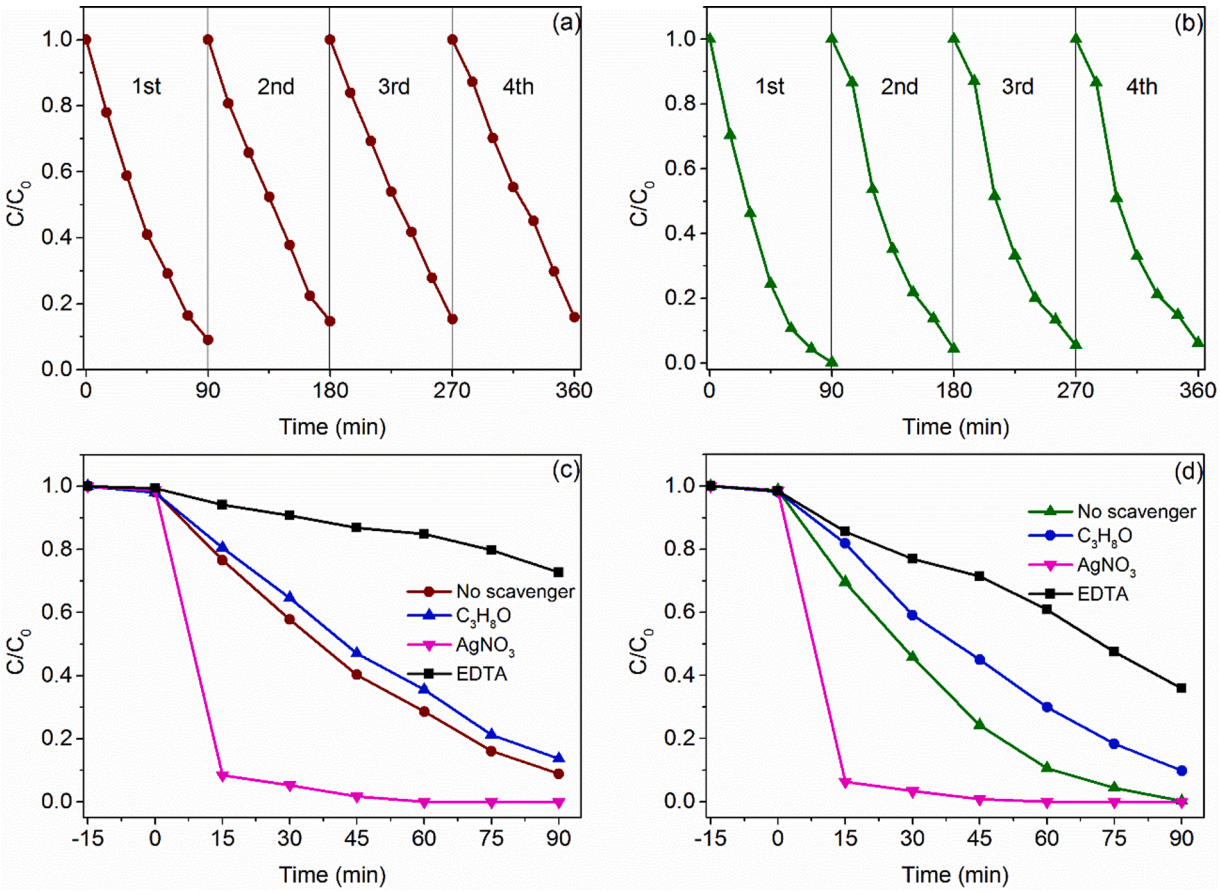

Fig. 5. (a) Recycling experiment for Nb_2O_5, (b) recycling experiment for Nb_2O_5/TiO_2, (c) RhB dye concentration variation using scavengers for Nb_2O_5, and (d) for Nb_2O_5/TiO_2.

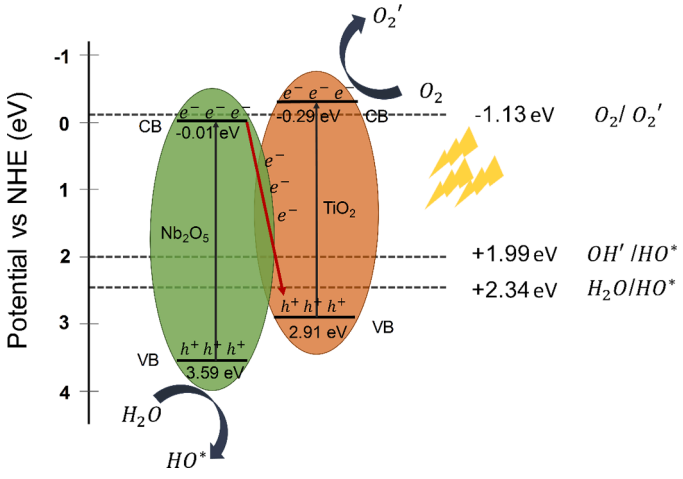

Fig. 6. Possible charge transfer mechanism.

material, electron/hole pairs (e^-/h^+) are generated. In this case, it is believed that the photogenerated e^- in Nb_2O_5, which has a lower reduction capacity, recombine with the photogenerated h^+ in the TiO_2 semiconductor, which has a lower oxidation potential, causing the oxidation and reduction reactions to take place in the semiconductor TiO_2. materials that have greater oxidizing and reducing capacities [53–57]. This mechanism of e^- transfer from the CB of Nb_2O_5 to the VB of TiO_2 is suggested by having a system that has many intermediate states, which makes it possible to receive the photogenerated e^-. The intermediate states are characteristic of the material's crystallization through the MAH synthesis method and can be confirmed by the PL result. Thus, according to the scheme of Fig. 6, the e^- photogenerated in TiO_2, which has a higher reduction potential, can reduce the oxygen adsorbed into a superoxide radical, since it has a more positive potential than the reduction potential of $O_2/O_2^{'}$ (-0.13 eV vs NHE) [58]. The h^+ photogenerated in the VB of Nb_2O_5 reacts with the adsorbed water, forming $HO^*$and $H^{\cdot}$. radicals, due to having a more positive potential than 1.99 eV vs NHE, related to $OH^{'}/HO^*$, are also more positive than 2.34 eV vs NHE, related to the potential of H_2O/HO^* [58,59]. The HO^* radicals that have high oxidizing power react with the RhB dye, degrading into intermediate products, according to the author's published work [12].

Even though the semiconductors used in this work are well-known and widely used materials, the heterostructure of these two compounds has not yet been well explored, especially in heterogeneous photocatalysis processes. Some works approach the mixture of Nb_2O_5 with TiO_2 and apply it to the degradation of other organic compounds [20,60]. Table 1 presents a summary of works that explored the use of heterostructures based on Nb_2O_5, which were used to evaluate the

Table 1
Comparison of the photocatalytic performance of the Nb_2O_5 heterostructure.

Heterostructure	Dye	Time	Light	% Degradation	Refs.
Nb_2O_5/TiO_2	RhB	90 min	UVl	100%	This work
Nb_2O_5/TiO_2	MB	150 min	Visible	84%	[61]
g-C_3N_4/ Nb_2O_5	RhB	180 min	Visible	79%	[62]
g-C_3N_4/ Nb_2O_5	RhB	210 min	UV	~80%	[63]
Nb_2O_5/SnO_2	RhB	180 min	UV	~80%	[64]
CeO_2/Nb_2O_5	MB	150 min	UV	~80%	[65]
TiO_2/ Nb_2O_5	ACT	-	Visible	90.6%	[30]

degradation of known dyes, such as RhB and MB. One of our great differentials in relation to the others mentioned is the method of obtaining the heterostructure, which was all through MAH synthesis. From the results, we were able to see that this method makes it possible to obtain a heterostructure of Nb_2O_5/TiO_2 with a high discoloration capacity of the RhB dye, proving to be competitive in relation to the others.

4. Conclusion

The Nb_2O_5/TiO_2 heterostructure was obtained in a simple and fast way through the microwave-assisted hydrothermal method. Nb_2O_5 has the characteristic of presenting low crystallinity of the pseudohexagonal phase at lower temperatures, and, together with TiO_2, it presented a mixture with the anatase phase. The formation of Nb_2O_5/TiO_2 showed the formation of smaller particles on the surface of Nb_2O_5, which favored the photocatalytic activity of this material when compared to Nb_2O_5, where 90 min of analysis allowed the discoloration of 100% of RhB. Additionally, h^+ was the active species that most positively influenced photocatalysis for both samples. This indicates that the heterostructure synthesized under the conditions of this work proved to be a material with interesting properties for application in photocatalysis processes.

Conflicts of interest

The authors declare that they have no competing interests.

Acknowledgments

The authors are thankful for the financial support of Brazilian research financing institutions: CAPES, CNPq, FAPERGS – Process n° 17/2551-0000889-8 and 19/2551-0001974-2 – and FAPESP (FAPESP CEPID-finance code 2013/07296-2). We also thank the CEME-SUL FURG. This study was financed in part by the Coordenação de Aperfeiçoamento de Pessoal de Nível Superior–Brasil (CAPES) – Finance Code 001.

References

[1] R. Kumar, A. Umar, R. Kumar, M.S. Chauhan, G. Kumar, S. Chauhan, Spindle-like Co_3O_4-ZnO nanocomposites scaffold for hydrazine sensing and photocatalytic degradation of rhodamine B dye, Eng. Sci. 16 (2021) 288–300, https://doi.org/10.30919/es8d548.

[2] S.A. Kumar, M. Jarvin, S. Sharma, A. Umar, S.S.R. Inbanathan, N.P. Lalla, Facile and green synthesis of MgO nanoparticles for the degradation of victoria blue dye under UV irradiation and their antibacterial activity, ES Food Agrofor. (2021) 14–19, https://doi.org/10.30919/esfaf519.

[3] X. Shi, J. Hong, C. Wang, S. Kong, J. Li, D. Pan, J. Lin, Q. Jiang, Z. Guo, Preparation of Mg,N-co-doped lignin adsorbents for enhanced selectivity and high adsorption capacity of As (V) from wastewater, Particuology 58 (2021) 206–213, https://doi.org/10.1016/j.partic.2021.03.014.

[4] J. Hong, L. Kang, X. Shi, R. Wei, X. Mai, D. Pan, N. Naik, Z. Guo, Highly efficient removal of trace lead (II) from wastewater by 1,4-dicarboxybenzene modified Fe/Co metal organic nanosheets, J. Mater. Sci. Technol. 98 (2022) 212–218, https://doi.org/10.1016/j.jmst.2021.05.021.

[5] Z. Deng, S. Sun, H. Li, D. Pan, R.R. Patil, Z. Guo, I. Seok, Modification of coconut shell-based activated carbon and purification of wastewater, Adv. Compos. Hybrid Mater. 4 (2021) 65–73, https://doi.org/10.1007/s42114-021-00205-4.

[6] Y. Liao, Y. Wang, L. Ouyang, Y. Dong, J. Zhou, Q. Hu, B. Qiu, Conductive polyaniline enhanced decolorization of azo dyes in anaerobic wastewater treatment, ES Food Agrofor. (2021) 35–42, https://doi.org/10.30919/esfaf584.

[7] Z. Sun, K. Qu, Y. Cheng, Y. You, Z. Huang, A. Umar, Y.S.A. Ibrahim, H. Algadi, L. Castañeda, H.A. Colorado, Z. Guo, Corncob-derived activated carbon for efficiently adsorption dye in sewage, ES Food Agrofor. (2021) 61–73, https://doi.org/10.30919/esfaf473.

[8] H. Zhang, X. Ding, S. Wang, Y. Huang, X. Zeng, S. Maganti, Q. Jiang, M. Huang, Heavy metal removal from wastewater by a polypyrrole- derived N-doped carbon nanotube decorated with fish scale- like molybdenum disulfide nanosheets, Eng. Sci. (2022) 1–9, https://doi.org/10.30919/es8d649.

[9] R. Nandanwar, J. Bamne, N. Singh, P.K. Sharma, P. Singh, A. Umar, F.Z. Haque, Synthesis of Titania/Silica nanocomposite for enhanced photodegradation of methylene blue and methyl orange dyes under UV and mercury lights, ES Mater. Manuf. (2022) 78–88, https://doi.org/10.30919/esmm5f628.

[10] B. Yuan, L. Li, V. Murugadoss, S. Vupputuri, J. Wang, N. Alikhani, Z. Guo, Nanocellulose-based composite materials for wastewater treatment and waste-oil remediation, ES Food Agrofor. (2020) 41–52, https://doi.org/10.30919/esfaf0004.

[11] M. Cheng, C. Yao, Y. Su, J. Liu, L. Xu, J. Bu, H. Wang, S. Hou, Cyclodextrin modified graphene membrane for highly selective adsorption of organic dyes and copper (II) ions, Eng. Sci. (2021) 299–307, https://doi.org/10.30919/es8d603.

[12] C.L. Ücker, F.C. Riemke, N.F. de Andrade Neto, A. de A.G. Santiago, T. J. Siebeneichler, N.L.V. Carreño, M.L. Moreira, C.W. Raubach, S. Cava, Influence of Nb_2O_5 crystal structure on photocatalytic efficiency, Chem. Phys. Lett. 764 (2021), https://doi.org/10.1016/j.cplett.2020.138271.

[13] D.R. Shinde, I.S. Quraishi, R.A. Pawar, An efficient visible light driven photocatalytic removal of dyes from the dye effluent using metal halide lamp based slurry reactor, ES Energy Environ. (2021) 54–62, https://doi.org/10.30919/esee8c504.

[14] C.L. Ücker, V. Goetzke, S.R. Almeida, E.C. Moreira, M.M. Ferrer, P.L.G. Jardim, M. L. Moreira, C.W. Raubach, S. Cava, Photocatalytic degradation of rhodamine B using Nb_2O_5 synthesized with different niobium precursors: factorial design of experiments, Ceram. Int. 47 (2021) 20570–20578, https://doi.org/10.1016/j.ceramint.2021.04.066.

[15] R.R.M. Silva, J.A. Oliveira, L.A.M. Ruotolo, A.L.A. Faria, C. Ribeiro, F.G. E. Nogueira, Unveiling the role of peroxo groups in Nb_2O_5 photocatalytic efficiency under visible light, Mater. Lett. 273 (2020), 127915, https://doi.org/10.1016/j.matlet.2020.127915.

[16] V.P. Letswalo, L.N. Dlamini, S.P. Malinga, A 2D/1D g-C_3N_4/Nb_2O_5 heterostructure in HPEI template with the potential for water treatment, Mater. Lett. X. 12 (2021), 100100, https://doi.org/10.1016/j.mlblux.2021.100100.

[17] B. Boruah, R. Gupta, J.M. Modak, G. Madras, Enhanced photocatalysis and bacterial inhibition in Nb_2O_5: via versatile doping with metals (Sr, Y, Zr, and Ag): A critical assessment, Nanoscale Adv. 1 (2019) 2748–2760, https://doi.org/10.1039/c9na00305c.

[18] A. Enesca, L. Andronic, The influence of photoactive heterostructures on the photocatalytic removal of dyes and pharmaceutical active compounds: a mini-review, Nanomaterials 10 (2020) 1–22, https://doi.org/10.3390/nano10091766.

[19] S. Das, J. Pérez-Ramírez, J. Gong, N. Dewangan, K. Hidajat, B.C. Gates, S. Kawi, Core-shell structured catalysts for thermocatalytic, photocatalytic, and electrocatalytic conversion of CO_2, Chem. Soc. Rev. 49 (2020) 2937–3004, https://doi.org/10.1039/c9cs00713j.

[20] J. Yan, G. Wu, N. Guan, L. Li, Nb_2O_5/TiO_2 heterojunctions: synthesis strategy and photocatalytic activity, Appl. Catal. B Environ. 152–153 (2014) 280–288, https://doi.org/10.1016/j.apcatb.2014.01.049.

[21] C.L. Ücker, V. Goetzke, F.C. Riemke, M.L. Vitale, L.R.Q. de Andrade, M.D. Ücker, E. C. Moreira, M.L. Moreira, C.W. Raubach, S.S. Cava, Multi-photonic behavior of Nb_2O_5 and its correlation with synthetic methods, J. Mater. Sci. (2021), https://doi.org/10.1007/s10853-021-05770-z.

[22] P. Chen, J. Peng, C. Liao, P.S. Shen, P.L. Kuo, Microwave-assisted hydrothermal synthesis of TiO_2 spheres with efficient photovoltaic performance for dye-sensitized solar cells, J. Nanopart. Res. 15 (2013) 1–11, https://doi.org/10.1007/s11051-013-1465-0.

[23] C. Qiang, N. Li, S. Zuo, Z. Guo, W. Zhan, Z. Li, J. Ma, Microwave-assisted synthesis of $RuTe_2$/black TiO_2 photocatalyst for enhanced diclofenac degradation: performance, mechanistic investigation and intermediates analysis, Sep. Purif. Technol. 283 (2022), 120214, https://doi.org/10.1016/j.seppur.2021.120214.

[24] S.Y. Mendiola-Alvarez, J. Araña, J.M. Doña Rodríguez, A. Hernández-Ramírez, G. Turnes Palomino, C. Palomino Cabello, L. Hinojosa-Reyes, Comparison of photocatalytic activity of αFe_2O_3-TiO_2/P on the removal of pollutants on liquid and gaseous phase, J. Environ. Chem. Eng. 9 (2021), https://doi.org/10.1016/j.jece.2020.104828.

[25] C. Hou, J. Hou, H. Zhang, Y. Ma, X. He, W. Geng, Q. Zhang, Facile synthesis of $LiMn_{0.75}Fe_{0.25}PO_4$/C nanocomposite cathode materials of lithium-ion batteries through microwave sintering, Eng. Sci. 11 (2020) 36–43, https://doi.org/10.30919/es5e1006.

[26] F. Zhang, W. Cheng, Z. Yu, S. Ge, Q. Shao, D. Pan, B. Liu, X. Wang, Z. Guo, Microwave hydrothermally synthesized WO_3/UiO-66 nanocomposites toward enhanced photocatalytic degradation of rhodamine B, Adv. Compos. Hybrid Mater. 4 (2021) 1330–1342, https://doi.org/10.1007/s42114-021-00346-6.

[27] R. Wang, S. Li, P. Hu, S. Chen, J. Wang, Densification Behavior and microstructure evolution of Mo manocrystals by microwave sintering, ES Mater. Manuf. (2021) 97–105, https://doi.org/10.30919/esmm5f433.

[28] W. Cheng, Y. Wang, S. Ge, X. Ding, Z. Cui, Q. Shao, One-step microwave hydrothermal preparation of Cd/Zr-bimetallic metal–organic frameworks for enhanced photochemical properties, Adv. Compos. Hybrid Mater. 4 (2021) 150–161, https://doi.org/10.1007/s42114-020-00199-5.

[29] R. Khatoon, S. Rauf, M. Ul Haq, S. Attique, S.U. Din, N. Ali, Y. Guo, H. Chen, Y. Tian, J. Lu, Design of highly sensitive and selective ethanol sensor based on α-Fe_2O_3/Nb_2O_5 heterostructure, Nanotechnology 32 (2021), https://doi.org/10.1088/1361-6528/abdd5e.

[30] X. Bi, G. Du, A. Kalam, D. Sun, W. Zhao, Y. Yu, Q. Su, B. Xu, A.G. Al-Sehemi, Constructing anatase TiO_2/Amorphous Nb_2O_5 heterostructures to enhance photocatalytic degradation of acetaminophen and nitrogen oxide, J. Colloid Interface Sci. 601 (2021) 346–354, https://doi.org/10.1016/j.jcis.2021.05.120.

[31] R. Li, J. Xu, Z. Lv, W. Dong, F. Huang, Achieving highly stable Sn-based anode by a stiff encapsulation heterostructure, Sci. China Mater. 65 (2022) 695–703, https://doi.org/10.1007/s40843-021-1783-0.

[32] J. Yan, T. Wang, S. Qiu, Z. Song, W. Zhu, X. Liu, J. Lian, C. Sun, H. Li, Insights into the efficient charge separation over Nb_2O_5/2D-C_3N_4 heterostructure for

exceptional visible-light driven H_2 evolution, J. Energy Chem. 65 (2022) 548–555, https://doi.org/10.1016/j.jechem.2021.06.030.
[33] S. Sharma, S. Kumar, S.M. Arumugam, M. Palanisami, V. Shanmugam, S. Elumalai, Nb_2O_5/g-C_3N_4 heterojunction facilitates 2,5-diformylfuran production via photocatalytic oxidation of 5-hydroxymethylfurfural under direct sunlight irradiation, ChemPhotoChem 6 (2022), https://doi.org/10.1002/cptc.202100199.
[34] H. Chen, J. Wang, Y. Zhao, Q. Zeng, G. Zhou, M. Jin, Three-dimensionally ordered macro/mesoporous Nb_2O_5/Nb_4N_5 heterostructure as sulfur host for high-performance lithium/sulfur batteries, Nanomaterials 11 (2021) 0–7, https://doi.org/10.3390/nano11061531.
[35] L. Wolski, O.I. Lebedev, C.P. Harmer, K. Kovnir, H. Abdelli, T. Grzyb, M. Daturi, M. El-Roz, Unraveling the origin of photocatalytic deactivation in CeO_2/Nb_2O_5 heterostructure systems during methanol oxidation: insight into the role of cerium species, J. Phys. Chem. C 125 (2021) 12650–12662, https://doi.org/10.1021/acs.jpcc.1c02812.
[36] B. Hao, J. Guo, L. Zhang, H. Ma, Magnetron sputtered TiO_2/CuO heterojunction thin films for efficient photocatalysis of Rhodamine B, J. Alloy. Compd. 903 (2022), 163851, https://doi.org/10.1016/j.jallcom.2022.163851.
[37] V. Goetzke, C.L. Ücker, L.T. Gularte, C.D. Fernandes, M.L. Moreira, S. da Silva Cava, P.L.G. Jardim, R. Camaratta, C.W. Raubach, A statistical study of assembly parameter modifications effects on the photovoltaic response of dye-sensitized solar cells, J. Electron. Mater. 50 (2021) 6149–6158, https://doi.org/10.1007/s11664-021-09136-8.
[38] C.L. Ücker, L.T. Gularte, C.D. Fernandes, V. Goetzke, E. Ceretta, C.W. Raubach, M. L. Moreira, S.S. Cava, Investigation of the properties of niobium pentoxide for use in dye-sensitized solar cells, J. Am. Ceram. Soc. 102 (2019) 1884–1892, https://doi.org/10.1111/jace.16080.
[39] J.E. Boschker, T. Markurt, M. Albrecht, J. Schwarzkopf, Heteroepitaxial growth of T-Nb_2O_5 on $SrTiO_3$, Nanomaterials 8 (2018) 895.
[40] D. Dambournet, I. Belharouak, K. Amine, Tailored preparation methods of TiO_2 anatase, rutile, brookite : mechanism of formation and electrochemical properties †, Chem. Mater. 22 (2010) 1173–1179, https://doi.org/10.1021/cm902613h.
[41] O.F. Lopes, V.R. De Mendonça, F.B.F. Silva, E.C. Paris, C. Ribeiro, Óxidos de Nióbio: Uma visão sobre a síntese do Nb_2O_5 e sua aplicação em Fotocatálise Heterogênea, Quim. Nova 38 (2015) 106–117, https://doi.org/10.1590/S0100-40422010000800018.
[42] A. León, P. Reuquen, C. Garín, R. Segura, P. Vargas, P. Zapata, P.A. Orihuela, FTIR and Raman characterization of TiO_2 nanoparticles coated with polyethylene glycol as carrier for 2-methoxyestradiol, Appl. Sci. 7 (2017) 1–9, https://doi.org/10.3390/app7010049.
[43] V.R. de Mendonça, W. Avansi, R. Arenal, C. Ribeiro, A building blocks strategy for preparing photocatalytically active anatase TiO_2/rutile SnO_2 heterostructures by hydrothermal annealing, J. Colloid Interface Sci. 505 (2017) 454–459, https://doi.org/10.1016/j.jcis.2017.06.024.
[44] G. Gohari, A. Mohammadi, A. Akbari, S. Panahirad, M.R. Dadpour, V. Fotopoulos, S. Kimura, Titanium dioxide nanoparticles (TiO_2 NPs) promote growth and ameliorate salinity stress effects on essential oil profile and biochemical attributes of Dracocephalum moldavica, Sci. Rep. 10 (2020) 1–14, https://doi.org/10.1038/s41598-020-57794-1.
[45] M. Ziolek, I. Sobczak, P. Decyk, L. Wolski, The ability of Nb_2O_5 and Ta_2O_5 to generate active oxygen in contact with hydrogen peroxide, Catal. Commun. 37 (2013) 85–91.
[46] M. Ristić, S. Popović, S. Musić, Sol-gel synthesis and characterization of Nb_2O_5 powders, Mater. Lett. 58 (2004) 2658–2663, https://doi.org/10.1016/j.matlet.2004.03.041.
[47] I.M. Iani, V. Teodoro, N.L. Marana, U. Coleto, J.R. Sambrano, A.Z. Simões, M. D. Teodoro, E. Longo, L.A. Perazolli, R.A.C. Amoresi, M. Aparecida Zaghete, Cation-exchange mediated synthesis of hydrogen and sodium titanates heterojunction: theoretical and experimental insights toward photocatalyic mechanism, Appl. Surf. Sci. 538 (2021), 148137, https://doi.org/10.1016/j.apsusc.2020.148137.
[48] A.A.G. Santiago, E.M. Macedo, F.K.F. Oliveira, R.L. Tranquilin, M.D. Teodoro, E. Longo, F.V. Motta, M.R.D. Bomio, Enhanced photocatalytic activity of $CaMoO_4$/g-C_3N_4 composites obtained via sonochemistry synthesis, Mater. Res. Bull. 146 (2022), 111621, https://doi.org/10.1016/j.materresbull.2021.111621.
[49] S.M. Lam, J.C. Sin, I. Satoshi, A.Z. Abdullah, A.R. Mohamed, Enhanced sunlight photocatalytic performance over Nb_2O_5/ZnO nanorod composites and the mechanism study, Appl. Catal. A Gen. 471 (2014) 126–135, https://doi.org/10.1016/j.apcata.2013.12.001.
[50] Y. Huang, F. Mei, J. Zhang, K. Dai, G. Dawson, Construction of 1D/2D W18O49/Porous g-C_3N_4 S-scheme heterojunction with enhanced photocatalytic H_2 evolution, Acta Phys. Chim. Sin. 38 (2021), https://doi.org/10.3866/pku.whxb202108028, 2108028–0.
[51] F. Mei, Z. Li, K. Dai, J. Zhang, C. Liang, Step-scheme porous g-C_3N_4/$Zn_{0.2}Cd_{0.8}$S-DETA composites for efficient and stable photocatalytic H_2 production, Chin. J. Catal. 41 (2020) 41–49, https://doi.org/10.1016/S1872-2067(19)63389-9.
[52] R.G. Pearson, Absolute electronegativity and hardness: application to inorganic chemistry ralph, Inorg. Chem. (1997) 734–740.
[53] X. Ke, J. Zhang, K. Dai, K. Fan, C. Liang, Integrated S-scheme heterojunction of amine-functionalized 1D CdSe nanorods anchoring on ultrathin 2D $SnNb_2O_6$ nanosheets for robust solar-driven CO_2 conversion, Sol. RRL. 5 (2021), 2000805, https://doi.org/10.1002/solr.202000805.
[54] X. Li, J. Zhang, Y. Huo, K. Dai, S. Li, S. Chen, Two-dimensional sulfur- and chlorine-codoped g-C_3N_4/CdSe-amine heterostructures nanocomposite with effective interfacial charge transfer and mechanism insight, Appl. Catal. B Environ. 280 (2021), 119452, https://doi.org/10.1016/j.apcatb.2020.119452.
[55] X. Li, J. Zhang, K. Dai, K. Fan, C. Liang, $Cd_3(C_3N_3S_3)_2$ polymer Sn schottky heterojunction for broadband-solar highly selective photocatalytic CO_2 reduction, Sol. RRL. 5 (2021), 2100788, https://doi.org/10.1002/solr.202100788.
[56] Z. Zhao, X. Li, K. Dai, J. Zhang, G. Dawson, *In-situ* fabrication of Bi_2S_3/$BiVO_4$/$Mn_{0.5}Cd_{0.5}$S-DETA ternary S-scheme heterostructure with effective interface charge separation and CO_2 reduction performance, J. Mater. Sci. Technol. 117 (2022) 109–119, https://doi.org/10.1016/j.jmst.2021.11.046.
[57] T. Hu, K. Dai, J. Zhang, S. Chen, Noble-metal-free Ni_2P modified step-scheme $SnNb_2O_6$/CdS-diethylenetriamine for photocatalytic hydrogen production under broadband light irradiation, Appl. Catal. B Environ. 269 (2020), 118844, https://doi.org/10.1016/j.apcatb.2020.118844.
[58] T. Cheng, H. Gao, R. Li, S. Wang, Z. Yi, H. Yang, Flexoelectricity-induced enhancement in carrier separation and photocatalytic activity of a photocatalyst, Appl. Surf. Sci. 566 (2021), 150669, https://doi.org/10.1016/j.apsusc.2021.150669.
[59] H. Ge, F. Xu, B. Cheng, J. Yu, W. Ho, S-scheme heterojunction TiO_2/CdS nanocomposite nanofiber as H_2-production photocatalyst, ChemCatChem 11 (2019) 6301–6309, https://doi.org/10.1002/cctc.201901486.
[60] A.M. Ferrari-Lima, R.G. Marques, M.L. Gimenes, N.R.C. Fernandes-Machado, Synthesis, characterisation and photocatalytic activity of N-doped TiO_2-Nb_2O_5 mixed oxides, Catal. Today 254 (2015) 119–128, https://doi.org/10.1016/j.cattod.2015.02.031.
[61] N.P. Ferraz, F.C.F. Marcos, A.E. Nogueira, A.S. Martins, M.R.V Lanza, E.M. Assaf, Y. J.O. Asencios, Hexagonal-Nb_2O_5/Anatase-TiO_2 mixtures and their applications in the removal of methylene blue dye under various conditions, Mater. Chem. Phys. 198 (2017) 331–340.
[62] G.T.S.T. Silva, K.T.G. Carvalho, O.F. Lopes, C. Ribeiro, Environmental g-C_3N_4/Nb_2O_5 heterostructures tailored by sonochemical synthesis : enhanced photocatalytic performance in oxidation of emerging pollutants driven by visible radiation, Appl. Catal. B Environ. 216 (2017) 70–79, https://doi.org/10.1016/j.apcatb.2017.05.038.
[63] K.T.G. Carvalho, A.E. Nogueira, O.F. Lopes, G. Byzynski, C. Ribeiro, Synthesis of g-C_3N_4/Nb_2O_5 heterostructures and their application in the removal of organic pollutants under visible and ultraviolet irradiation, Ceram. Int. 43 (2017) 3521–3530, https://doi.org/10.1016/j.ceramint.2016.11.063.
[64] T.A. Rodrigues, P.H.E. Falsetti, D.M.S. Del Duque, G.T.S.T. da Silva, O.F. Lopes, W. Avansi, C. Ribeiro, V.R. de Mendonça, A versatile Nb_2O_5/SnO_2 heterostructure for different environmental purposes: water treatment and artificial photosynthesis, ChemCatChem 13 (2021) 730–738, https://doi.org/10.1002/cctc.202001569.
[65] N.P. Ferraz, A.E. Nogueira, F.C.F. Marcos, V.A. Machado, R.R. Rocca, E.M. Assaf, Y. J.O. Asencios, CeO_2–Nb_2O_5 photocatalysts for degradation of organic pollutants in water, Rare Met. 39 (2019) 230–240, https://doi.org/10.1007/s12598-019-01282-7.